Inorganic Chemistry

Article

pubs.acs.org/IC

Multinary Selenides with Unusual Coordination Environment of Bismuth

Ming-Yan Chung and Chi-Shen Lee*

Department of Applied Chemistry, National Chiao Tung University, 1001 University Road, Hsinchu 30010, Taiwan

Supporting Information

ABSTRACT: New multinary selenides $Ae_3SnPn_2Se_8$ (Ae = Sr, Ba; Pn = Sb, Bi), $Sr_{8.01}Ge_{2.04}Bi_{7.95}Se_{24}$, and $Sr_8YGe_2Bi_7Se_{24}$ were synthesized by solid-state reaction, and their structures were determined by single-crystal X-ray diffraction. These compounds crystallize in orthorhombic space group *Pnma* (no. 62) for $Ae_3SnPn_2Se_8$ (Ae = Sr, Ba; Pn = Sb, Bi) and in $Pna2_1$ (no. 33) for $Sr_{8.01}Ge_{2.04}Bi_{7.95}Se_{24}$ and $Sr_8YGe_2Bi_7Se_{24}$. The structures feature one-dimensional corner sharing tetrahedral $^1_\infty[MSe_3]$ units, and one-dimensional edge sharing octahedral $^1_\infty[M_4Se_{10}]$, packed with the alkaline earth or rare earth cations. $Sr_{8.01}Ge_{2.04}Bi_{7.95}Se_{24}$ and $Sr_8YGe_2Bi_7Se_{24}$ contain a triple cell superlattice structure derived from a special arrangement of Bi and Ge in the tetrahedrally coordinated $^1_\infty[MSe_3]$ chain. Diffuse reflectance spectra and electronic resistivity measurements indicate semiconducting behaviors; the $Sr_8YGe_2Bi_7Se_{24}$ Seebeck coefficient is −180 μV/K at 303 K. Electronic structure calculations confirm that the electron count for $Sr_8YGe_2Bi_7Se_{24}$ is optimal for interatomic bonding in the ionic network.

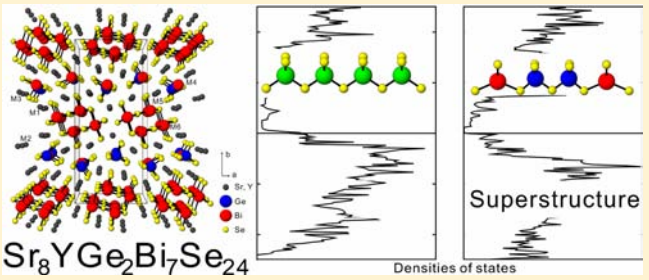

1. INTRODUCTION

Metal chalcogenides show a rich structural diversity and have unusual physical and chemical properties, which have been the subject of intensive research for applications in solar energy conversion[1] and thermal electrics.[2−5] Among these materials, multinary chalcogenides with alkali, alkaline earth, and rare earth elements are of particular interest.[2−4] Incorporating large cations reduces chalcogenide dimensionality, which is expected to reduce thermal conductivity resulting from ionic interactions between the cation and chalcogen anions, so enhancing thermoelectric properties.[4] Ternary metal chalcogenides incorporated into thermoelectric devices have applications in energy conversion and infrared detection.[1,2,4] Many new metal chalcogenide phases have appeared during the past decades, which we can summarize as the A/M/Q (A = alkali, alkaline earth, or rare earth metal; M = group 3−5 p-block metal; Q = S, Se, Te) systems.

The structural chemistries of multinary pnictides and tetrelides are interesting due to significant stereochemical activity, which gives a variety of coordination complexes of Pn (Pn = Sb, Bi) and Tt (Tt = Ge, Sn). For alkaline metal chalcogenides, the $A_m[M_{1+l}Se_{2+l}]_{2m}[M_{2l+n}Se_{2+3l+n}]$ (A = K, Cs, Rb, Sr, Ba; M = M, M′ main group element) homologous series shows an interesting structural relationship.[6−9] $CsBi_4Te_6$ exhibits good thermoelectric properties at 200 K (figure of merit, ZT ∼ 0.8),[3] which contains Cs atoms located in the interlayer of Bi_2Te_3 blocks to form a complex structure type. For alkali and alkaline earth chalcogenides, many ternaty/quaternary phases in $AMBiS_4$ and Ae/M/Q systems ((A = Rb, Cs; Ae = Sr, Ba; M = group 14/15 elements; Q = Se; Te) were investigated.[10−17] These compounds contain varies coordination geometries of main group cations and polychalcogens anion units. For lanthanide chalcogenides, quaternary sulfide and selenide $La_4FeSb_2Q_{10}$ (Q = S, Se)[18] with unique 4-coordinated Sb environments were reported. Multinary chalcogenides in A/M/Q (A = alkaline, alkaline earth, lanthanide; M = M, M′ main group element; Q = S, Se, Te), such as $A_2Bi_4Se_7$ (A = Rb, Cs),[19] Ae_2TtQ_4 (Ae = Sr, Ba, Eu; Tt = Ge, Sn; Q = S, Se),[20−22] $A_2Bi_8Se_{13}$ (A = Cs, Rb), A_4TtQ_4 (A = K, Rb; Tt = Ge, Sn; Q = S, Se),[23,24] and $La_3Tt_{1.25}S_7$ (Tt = Ge, Sn)[25] etc., have been investigated during the past decade.

Because of the rich diversity of chalcogenide phases, and the possibility of these compounds bearing favorable thermoelectric properties, the Ae/Tt/Pn/Q (Q = S, Se) systems were targeted for synthesis of new phases, with unique structure and properties. This paper presents part of our systematic investigation into multinary chalcogenides. Our previous work in the selenide system revealed a new quaternary phase, $Sr_3GeSb_2Se_8$.[26] In this study, we extend this system to search for new analogues with the general formula "$Ae_3TtPn_2Se_8$" (Ae = Sr, Ba; Tt = Ge, Sn; Pn = Sb, Bi). Here, we present five new multinary selenides for the first time. The general structural building blocks for these new phases are similar to that of the previously reported $Sr_3GeSb_2Se_8$.[26] Moreover, we isolated two compounds with a superlattice structure with an unusual coordination environment for the Bi atom. We determined the electronic structures of these selenides from electronic structure calculations, which subsequently informed the synthesis of $Sr_8YGe_2Bi_7Se_{24}$.

Received: September 18, 2012
Published: December 3, 2012

   dx.doi.org/10.1021/ic302027b | *Inorg. Chem.* 2012, 51, 13328−13333

Table 1. Crystal Data and Conditions of Data Collection for I–V

	I	II	III	IV	V
refined composition	$Sr_{8.007(4)}Ge_{2.043(4)}Bi_{7.949(8)}Se_{24}$	$Sr_8YGe_2Bi_7Se_{24}$	$Sr_3Sn_{0.96(9)}Bi_{2.04(9)}Se_8$	$Ba_{3.00(4)}SnSb_2Se_8$	$Ba_{3.00(1)}Sn_{0.87(2)}Bi_{2.13(2)}Se_8$
temperature	273(2) K	273(2) K	273(2) K	273(2) K	273(2) K
wavelength	0.71073 Å	0.71073 Å	0.71073 Å	0.71073 Å	0.71073 Å
crystal system	orthorhombic	orthorhombic	orthorhombic	orthorhombic	orthorhombic
space group, Z	$Pna2_1$ (33), 4	$Pna2_1$ (33), 4	$Pnma$ (62), 4	$Pnma$ (62), 4	$Pnma$ (62), 4
a/Å	12.8036(9)	12.835(2)	12.9745(7)	12.715(3)	13.125(3)
b/Å	29.016(2)	29.068(3)	4.2352(2)	4.5509(9)	4.4012(9)
c/Å	12.8192(9)	12.848(2)	29.092(2)	29.660(6)	29.823(6)
V/Å^3	4762.5(6)	4793(1)	1598.6(1)	1716.3(6)	1722.8(6)
θ_{min}, θ_{max}/deg	1.74, 25.13	1.40, 25.08	1.72, 25.09	1.37, 25.05	2.07, 28.28
independent reflections (R_{int})	8477 (0.0708)	8487 (0.0941)	1627 (0.0431)	2381 (0.0414)	2401 (0.0446)
observed reflections	43069	41421	14245	18927	19678
absorption coefficient/mm^{-1}	57.753	55.069	51.593	28.242	47.832
goodness-of-fit on F^2	1.007	1.041	1.092	1.090	1.045
R_1, wR_2 ($I > 2\sigma(I)$)	0.0451, 0.1129	0.0499, 0.1010	0.0354, 0.0908	0.0448, 0.1014	0.0379, 0.0868
R_1, wR_2 (all data)[a]	0.0851, 0.1362	0.1150, 0.1256	0.0373, 0.0920	0.0560, 0.1092	0.0434, 0.0903
largest diff. peak and hole/eÅ^{-3}	2.002, −3.757	4.611, −3.849	3.862, −4.348	2.464, −3.666	5.959, −5.739

[a] $R_1 = \sum||F_0| - |F_c||/\sum|F_0|$. $wR_2 = \{\sum[w(F_0^2 - F_c^2)^2]/\sum[w(F_0^2)^2]\}^{1/2}$.

2. EXPERIMENTAL SECTION

2.1. Synthesis. All operations on compounds were performed in a glovebox with a dry nitrogen atmosphere. Chemicals were used as obtained (from Alfa Aesar)—Ba, 99.00%, chunks; Sr, 99.00%, chunks; Ge, 99.50%, powder; Sn, 99.80%, powder; Sb, 99.90%, powder; Bi, 99.50%, powder; Se, 99.95%, powder; Y, 99.00%, chunks; La, 99.00%, chunks.

Initially, $Ae_3TtPn_2Q_8$ (Ae = Ca, Sr, Ba; Tt = Ge, Sn; Pn = Sb, Bi; Q = S, Se) were carried out to synthesize analogues of $Sr_3GeSb_2Se_8$.[26] In a typical reaction, stoichiometric proportions of the pure elements were mixed in an N_2-filled glovebox (total mass ~0.5 g), placed in a carbon-coated silica tube,[27] sealed under dynamic vacuum, and slowly heated to 1023 K over 48 h. This temperature was maintained for one day, followed by slow cooling to 673 K at a rate of 15 K/h, and finally to about 300 K (room temperature) by simply terminating the power.

In general, these reactions yielded polycrystalline ingots with a metallic luster. Powder X-ray diffraction measurements of reaction products for $Ba_3SnBi_2Se_8$, $Ba_3SnSb_2Se_8$, $Sr_3SnBi_2Se_8$, and $Sr_3GeBi_2Se_8$ showed similar patterns to that of $Sr_3GeSb_2Se_8$. The products were separated into small samples, from which suitable samples for single-crystal X-ray diffraction were selected. Structural determinations confirmed the formulas as $Sr_{8.01}Ge_{2.04}Bi_{7.95}Se_{24}$ (**I**), $Sr_8YGe_2Bi_7Se_{24}$ (**II**), $Sr_3Sn_{0.96}Bi_{2.04}Se_8$ (**III**), $Ba_3SnSb_2Se_8$ (**IV**), and $Ba_3Sn_{0.87}Bi_{2.13}Se_8$ (**V**). Pure phases of **I**, **II**, **IV**, and **V** were directly synthesized by heating stoichiometric mixtures of elements under the same reaction conditions as described above.

The electronic structure calculations suggest a charge balanced model with general formula "$Ae_8ReTt_2Pn_7Q_{24}$" (Ae = Sr, Ba; Re = Y, La; Tt = Ge, Sn; Pn = Sb, Bi; Q = S, Se). Reactions derived from that formula were carried out, and we confirmed that a new quintet phase of $Sr_8YGe_2Bi_7Se_{24}$ (**II**) was successfully synthesized and characterized.

2.2. Characterization. Powder X-ray diffraction (PXRD) was carried out using a Bruker D8 Advance diffractometer (operated at 40 kV and 40 mA, Cu Kα, λ = 1.5418 Å). The PXRD data were obtained in a 2θ range from 5° to 60° using a 0.016° step size and 0.1 s/step exposure time. The unit cell parameters were examined by CELREF program utilizing PXRD patterns.[28] Diffuse reflectance measurements were performed at approximately 25 °C with a UV–visible spectrophotometer (Jasco V-570); an integrating sphere was used to measure the diffuse reflectance spectra over the range 200–2000 nm. Ground powder samples were pressed onto a thin glass slide holder, and a $BaSO_4$ plate served as reference. The band gap was determined by extrapolating the linear regions of each $(\alpha h\nu)^2$ versus energy plot to $(\alpha h\nu)^2$ to 0.[29] Analyses of as-synthesized crystalline samples with energy-dispersive spectra (SEM/EDX, Hitachi H-7500 Scanning Electron Microscope) showed the presence of constituent elements. Measurements of differential thermal analysis (DTA) were performed with a thermal analyzer (NETZSCH STA 409PC). Powder samples (approximately 40 mg) were sealed in silica capsules and placed in alumina crucibles. After heating to 1073 K with a rate of 10 K/min, the samples were cooled to 673 at 10 K/min under a constant flow of N_2. Electrical resistivity measurements were performed using the standard four-probe method on cold pressed bars (1 mm × 1 mm × 5 mm). The samples were annealed at 773 K for 6 days before the measurement. The Seebeck coefficient was measured on a cold-pressed bar (1 mm × 1 mm × 5 mm) using commercial thermopower measurement apparatus (MMR Technologies) in the temperature range 300–600 K under a dynamic vacuum (~10^{-2} Torr).

2.3. Single-Crystal X-ray Diffraction. Single crystals (~0.04 mm × 0.04 mm × 0.12 mm) obtained from products of the reactions of $Sr_3GeBi_2Se_8$, $Sr_8YGe_2Bi_7Se_{24}$, $Sr_3SnBi_2Se_8$, $Ba_3SnSb_2Se_8$, and $Ba_3SnBi_2Se_8$ were mounted on glass fibers with epoxy glue. Intensity single-crystal X-ray diffraction (SXRD) data were collected on a diffractometer of Bruker APEX CCD equipped with graphite-monochromated Mo Kα radiation (λ = 0.71073 Å). The distance from the crystal to the detector was 4.0 cm. The duration of exposure was 25 s/frame for $Ba_3SnBi_2Se_8$ and 40 s/frame for other samples. The 2θ values varied between 2.74° and 56.56°. Diffraction signals obtained from 200 frames of reciprocal-space images were utilized to determine unit-cell parameters. The APEX 2 program package was used for the structure determination and refinement.[30] Absorption corrections were based on fitting a function to the empirical transmission surface, as sampled by multiple equivalent measurements of numerous reflections. Further details of crystallographic analysis for all crystal data are available as the Supporting Information, and the results are listed in Tables 1, S1, and S2.

2.4. Calculation of Electronic Structure. Tight binding of linear muffin-tin orbitals (LMTO) with atomic sphere approximation (ASA) were undertaken to understand the electronic structure. In LMTO, we use density functional theory with local density approximation (LDA).[31–35] Three hypothetical models, $Sr_9Ge_3Bi_6Se_{24}$, $Sr_9Ge_2Bi_7Se_{24}$, and $Sr_8YGe_2Bi_7Se_{24}$ were constructed. The $Sr_9Ge_3Bi_6Se_{24}$ and $Sr_9Ge_2Bi_7Se_{24}$ models were obtained from the SXRD data of **I**, whereas the $Sr_8YGe_2Bi_7Se_{24}$ model was derived from the crystal structure of **II**. The k space integration was performed on a grid of more than 300 independent k-points. We analyzed the electronic structures using information from densities of states (DOS) and crystal orbital-Hamiltonian population (COHP) curves.[36]

dx.doi.org/10.1021/ic302027b | Inorg. Chem. 2012, 51, 13328–13333

2. RESULTS AND DISCUSSION

3.1. Synthesis and X-ray Powder Diffraction. Initially, SXRD analysis for **I** gave an unclear result with a formula $Sr_9Ge_{2.04}Bi_{6.96}Se_{24}$ (charge = −0.96/formula). To extend the study for the pure phase and analogue compounds, reactions with slightly different compositions were carried out and these reactions contained formula of deficient Se, deficient cations, interstitial cations, and constrained Ge/Bi composition for cation sites. Finally, pure phase of **I** was observed from the reaction "$Sr_{8.08}Ge_{2.10}Bi_{7.83}Se_{24}$," which suggests Bi and Sr atoms are mix-occupied. Subsequently, we successfully prepared single phases of **II**, **IV**, and **V**, while compound **III** could not be isolated in a pure state. The PXRD patterns of **I**, **II**, **IV**, and **V** are comparable to their theoretical patterns (Supporting Information Figure S1−S4).

3.2. Structural Description. *3.2.1. $Sr_{8.01}Ge_{2.04}Bi_{7.95}Se_{24}$ (I) and $Sr_8YGe_2Bi_7Se_{24}$ (II).* **I** and **II** crystallize in a novel structure type with the *Pna*2$_1$ space group, belonging to the family of $Sr_3GeSb_2Se_8$-related structures; this is best described as an ordered superstructure of $Sr_3GeSb_2Se_8$. To simplify the discussion, we use the structure of **II** as a representative and describe this structure in detail.

The structure is more complex than that of **III**, and the structure of **II** is shown in Figure 1a. The ionic network is made up of the same 1D chains as **III** is. However, the electron densities of metal sites in the $^1_\infty[MSe_3]$ 1D chain show significant differences. SXRD data indicate that the centers of the tetrahedral polyhedra contain bismuth and germanium at different sites. These are interlinked through corners to form a one-dimensional chain running along the *c*-axis. The $BiSe_4$ tetrahedra are further connected via two $GeSe_4$ tetrahedral units to form the 1D chain, $^1_\infty[(GeSe_3^{2-})(BiSe_3^{3-})(GeSe_3^{2-})]$, as shown in Figure 1b. The Bi and Ge positioning along the 1D chain is the reason that the super cell structure of **II** is three times larger than that of **III**. The local environment of tetrahedra $BiSe_4$ has two short contacts of approximately 2.70 Å and two remote contacts at about 2.90 Å. Tetrahedral $GeSe_4$ of similar structure has contacts ranging from 2.34 to 2.40 Å. To our knowledge, both the tetrahedral Bi coordination and special sequences of the 1D tetrahedral chains were first investigated in the chalcogenide system.

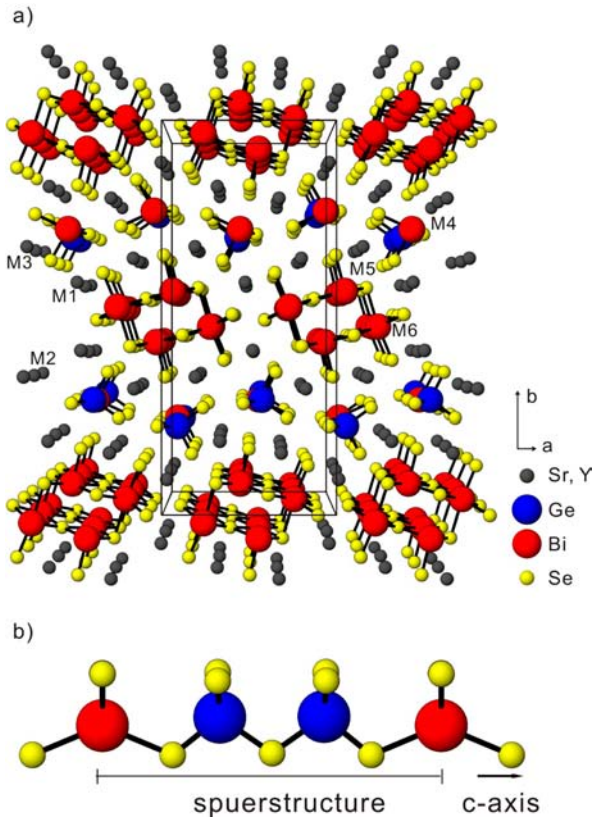

Figure 1. Crystal structure of **II** viewing down the *c*-axis [001] (a) and its superstructure, $^1_\infty[(GeSe_3^{2-})(BiSe_3^{3-})(GeSe_3^{2-})]$ (b).

The second unit, $^1_\infty[Bi_4Se_{10}^{8-}]$, is constructed from Bi(5A)−Bi(6C) octahedra. The Bi−Se contacts in the M(5A)−(6C) environment range from 2.71 to 3.10 Å, comparable to those of $SrBiSe_4$.[37] The ellipsoid plots of the first and second parts in **III** and **II** are illustrated in Supporting Information Figure S5. The third part, Sr (or Y), is coordinated to seven or eight Se atoms, forming monocapped or bicapped trigonal prismatic environments. The Sr−Se (or Y−Se) contacts range from 3.10 to 3.66 Å, comparable to those of $SrBiSe_4$[37] and $Y_3CuGeSe_7$.[38]

To investigate systematic differences between Bi atoms in tetrahedral and octahedral environments, the bond valence sums were calculated from Bi parameters for M(4B) and M(5A)−(6C) sites in **II** (Supporting Information Table S3). The values range from 3.15 to 3.33, close to the oxidation state of Bi^{3+}.

3.2.2. $Sr_3Sn_{0.96}Bi_{2.04}Se_8$ (III), $Ba_3SnSb_2Se_8$ (IV), and $Ba_3Sn_{0.87}Bi_{2.13}Se_8$ (V). **III**−**V** are isostructural with $Sr_3GeSb_2Se_8$.[26] Here we focus on **III** as their representative. The structure contains 14 crystallographic sites: there are distinct Sr atoms (Sr(1)−(3)), two for mixed occupancies of Sn and Bi (M(4), M(6)), one for Bi (M(5)), and eight for Se atom (Se(1)−(8)). The structure is illustrated in Figure 2a with a view along the *b*-axis. The ionic structure of **III** contains two types of one-dimensional units. The first type is made up of MSe_4 tetrahedral polyhedra interlinked through two corners to form one-dimensional chains $^1_\infty[MSe_3]$ that run along the *b*-axis (Figure 2b). The second type contains four MSe_6 octahedral units, fused to form an edge-shared $^1_\infty[M_4Se_{10}]$ unit; this type is also extended along the *b*-axis. One-dimensional chains of $^1_\infty[MSe_3]$ and $^1_\infty[M_4Se_{10}]$ units are parallel to the *a*-axis and form alternate layers of one-dimensional (1D) chains. Sr^{2+} cations fill the interstitial sites between these chains, similar to many alkali/alkaline earth chalcogenide compounds.[10,12,16]

The distinct Sr(1)−(3) sites are stable in a monocapped or bicapped trigonal prism environment with a Sr−Se range of 3.14−3.71 Å. The M(4) site has a distorted tetrahedral environment, comprising mixed-occupation by 86% Sn and 14% Bi, and is coordinated by four selenium atoms. The M-Se distances are in the range 2.46−2.77 Å, slightly larger than the Sn−Se contacts (2.47−2.62 Å),[39] indicative of a small Bi contribution. M(5) and M(6) are 100% Bi, and 86%/14% Bi/Sn, respectively. M(5) coordinates to three short (approximately 2.80 Å), two medium (approximately 3.06 Å), and one long (approximately 3.54 Å) M−Se distances, whereas the M(6) site is located in a distorted octahedral environment with an M(6)−Se distance in the range 2.75−3.05 Å. The M-Se contacts in M(5)−(6) sites are comparable to some multinary chalcogenide complexes, such as $EuBiSe_3$[40] and $Rb_2Bi_4Se_7$.[19]

3.3. Physical Properties. Optical properties for **I**, **II**, **IV**, and **V** were measured by UV−vis diffuse reflectance spectroscopy. We calculated the optical band gaps using the relation: $\alpha h\nu = A(h\nu - E_g)^m$, where *A* is a constant, $h\nu$ is the incident

dx.doi.org/10.1021/ic302027b | Inorg. Chem. 2012, 51, 13328−13333

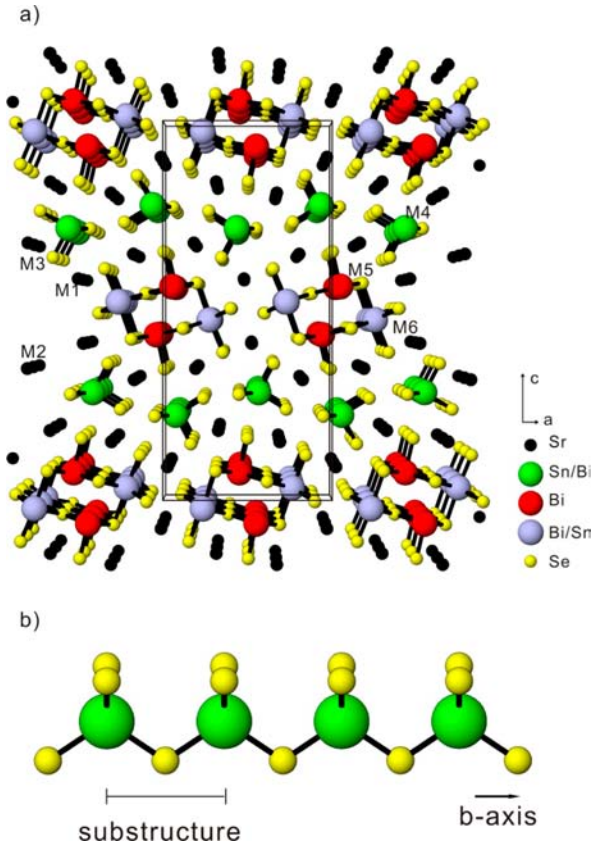

Figure 2. Crystal structures of **III** (a) in a projection along the *b*-axis [010] and its $^{1}_{\infty}[MSe_3]$ chains (b).

photon energy, and m = 0.5 and 2 for direct and indirect transitions, respectively.[29] Plots of $(\alpha h\nu)^2$ vs $h\nu$ are shown in Figure 3. The optical band gaps of **I**, **II**, **IV**, and **V** are 0.74, 0.70, 0.97, and 0.79 eV, respectively.

Supporting Information Figure S6 shows DTA curves versus temperature for **I**, **II**, **IV**, and **V**. The DTA measurements for these compounds share similar features, with exothermic absorption beginning at 1060, 1065, 970, and 1130 K for **I**, **II**, **IV**, and **V**, respectively, corresponding to the melting points of those compounds.

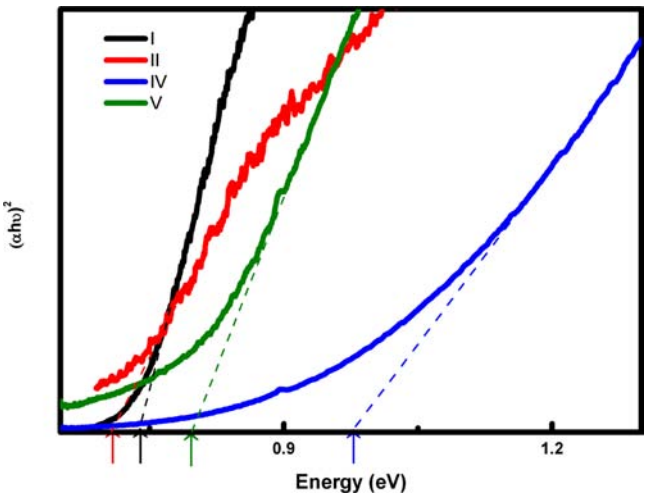

Figure 3. Plots of $(\alpha h\nu)^2$ vs photonenergy (eV) for **I** (black), **II** (red), **IV** (blue), and **V** (green).

The temperature dependence of **I**, **II**, **IV**, and **V** electronic resistivities were determined using the four probes method, in the temperature range 300−600 K (Figure 4). Resistivity

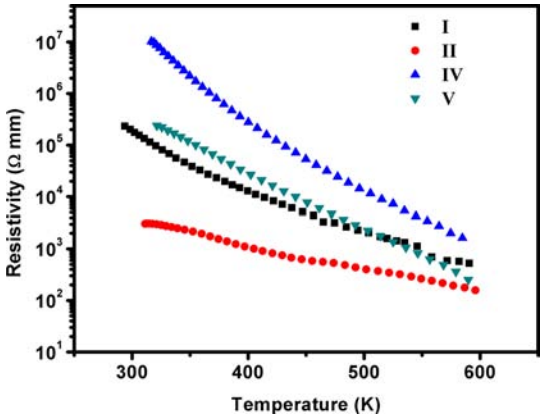

Figure 4. Temperature dependence of electrical resistivity of **I**, **II**, **IV**, and, **V**.

gradually increases with decreasing temperature for all phases, indicating semiconductor behavior. The calculated activation energies for **I**, **II**, **IV**, and **V** are respectively 0.41, 0.22, 0.51, and 0.67 eV, and this trend is consistent with our diffuse reflectance results.

Figure 5 is a plot of the Seebeck coefficient of **II** against temperature. We were unable to determine the coefficient of

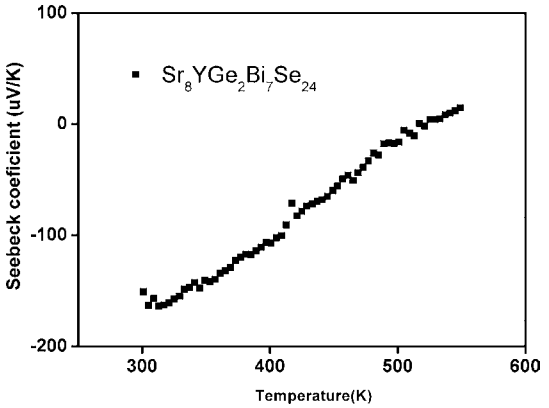

Figure 5. Temperature dependence of thermoelectric power of **II**.

the remaining compounds, due to their high resistivity exceeding the limitations of our instrument. **II** features negative Seebeck coefficients between 300 and 550 K, indicative of an *n*-type semiconductor.

3.4. Electronic Structure. To understand the electronic structure of these selenides, we derived three hypothetical models, $Sr_9Ge_3Bi_6Se_{24}$ (**1**), $Sr_9Ge_2Bi_7Se_{24}$ (**2**), and $Sr_8YGe_2Bi_7Se_{24}$ (**3**) with different occupancies at the main group metal positions (see Supporting Information Table S4).

For model **1**, the Fermi level (V_{ec} = 204 $e^-/[Sr_3GeBi_2Se_8]_3$) is close to the local minima of the total DOS (TDOS) and there is a nonzero contribution of electronic states at the Fermi level (Figure 6a), thus we could not model semiconducting properties from the electronic band-structure structure calculations. According to the COHP analysis, the Ge−Se bonding interactions are not optimal, and there is some antibonding character present.

dx.doi.org/10.1021/ic302027b | *Inorg. Chem.* 2012, 51, 13328−13333

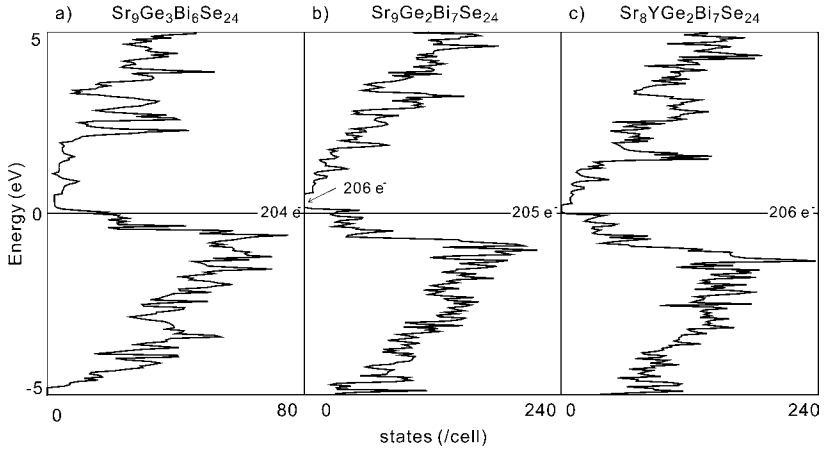

Figure 6. Densities of states for model $Sr_9Ge_3Bi_6Se_{24}$ (a), $Sr_9Ge_2Bi_7Se_{24}$ (b), and $Sr_8YGe_2Bi_7Se_{24}$ (c) in an energy window of 5 to −5 eV. The horizontal line denotes the Fermi energy (E_F), which is respectively 204, 205, and 206 e^-/formula for a, b, and c.

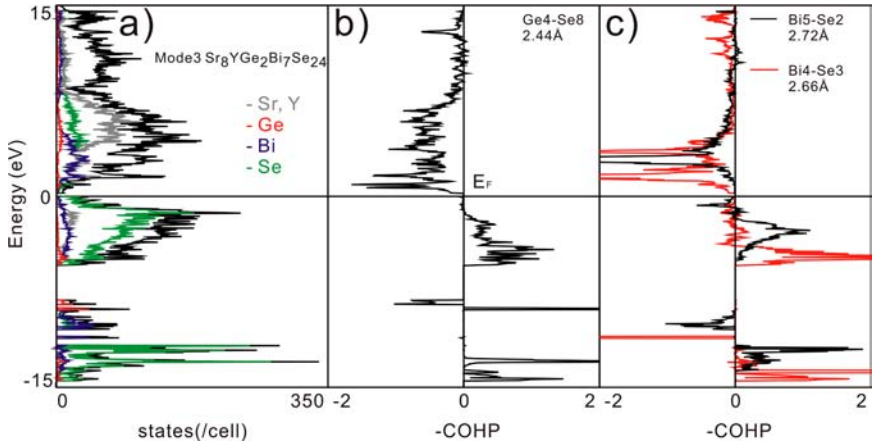

Figure 7. Densities of states (a) and crystal orbital Hamiltonian populations (COHP) plots for selected Ge−Se (b) and Bi−Se (c) contacts from model $Sr_8YGe_2Bi_7Se_{24}$. The horizontal line denotes the Fermi energy (E_F).

Model **2** features a triple cell structure with a formula of $Sr_9Ge_2Bi_7Se_{24}$, and the results are plotted in Figure 6b. It is clear that a band gap is present at 206 e^-/formula, which is one electron greater than for $Sr_9Ge_2Bi_7Se_{24}$ (205 e^-/formula). The result suggests that a hypothetical composition, providing 206 e^-/formula, such as $Sr_9GeBi_8Se_{24}$ (replacing Ge with Bi) or $Sr_8YGe_2Bi_7Se_{24}$ (replacing Sr with Y), will form a stable phase. Attempts to prepare these two compounds yielded instead the quintet phase $Sr_8YGe_2Bi_7Se_{24}$.

The $Sr_8YGe_2Bi_7Se_{24}$ DOS curve (Model **3**) is illustrated in Figures 6c and 7a. These plots reveal a clear band gap, with optimal valence elections, at 206 e^-/formula. The occupied DOS region contains several sections. The dominant valence band below −5 eV arises from the *n*s states of the main group elements, while the *n*p states mostly occur between −5 eV to the Fermi level. The conduction band contains primary Bi 5p, Sr 4d, Y 4d, and Se 4p states, hybridized with minor contributions from the Se 4s and Ge 3p states.

We investigated COHP curves to gain insight into the electronic characteristics of Ge−Se and Bi−Se coordination, shown in Figure 7b and c. The selected Ge−Se contact is essentially optimized. For the selected Bi4−Se contact, the weak interactions extend between −0 and −3.5 eV, distinct from typical Bi^{3+} interactions. For comparison, the Bi5−Se contact has some antibonding character in a range 0 to −1 eV, which may arise from localization of the lone-pair electrons on Bi. The −ICOHP values for Bi4−Se and Bi5−Se contacts are respectively 1.46 and 1.06 (eV/bond), indicative of greater bonding strength for Bi4−Se than is present in the Bi5−Se contacts. The Bi4 has shorter Bi−Se contacts than Bi5 does, resulting in greater bond energy. This confirms that such tetrahedral coordination stabilizes the Bi^{3+} ion.

4. CONCLUSIONS

Five new chalcogenides: $Sr_{8.01}Ge_{2.04}Bi_{7.95}Se_{24}$ (**I**), $Sr_8YGe_2Bi_7Se_{24}$ (**II**), $Sr_3Sn_{0.96}Bi_{2.04}Se_8$ (**III**), $Ba_3SnSb_2Se_8$ (**IV**), and $Ba_3Sn_{0.87}Bi_{2.13}Se_8$ (**V**) were prepared and characterized. These compounds contain one-dimensional building units, $^1_\infty[MeSe_3]$ and $^1_\infty[M_4Se_{10}]$, surrounded by alkaline earth, or rare earth, cations. The sequence $^1_\infty[(GeSe_3^{2-})(BiSe_3^{3-})(GeSe_3^{2-})]$ was observed in **I** and **II**. This novel one-dimensional structure contains a new tetrahedral Bi environment, which is responsible for the existence of a superlattice structure. Diffused reflectance spectral and electrical resistivity measurements indicated semiconductor behaviors for **I**, **II**, **IV**, and **V**. The Seebeck coefficient for **II** indicates *n*-type semiconductor behavior at room temperature. Electronic structure calculations suggest optimized bonding, and a bandgap at 206 e^-/formula. On the

dx.doi.org/10.1021/ic302027b | *Inorg. Chem.* 2012, 51, 13328−13333

basis of theoretical calculation, we successfully prepared the new quintet phase, **II**.

■ ASSOCIATED CONTENT

Supporting Information

(1) Crystallographic analysis of **I**–**V**, (2) experimental and simulated X-ray powder patterns for compounds **I**–**IV**, (3) elliposid plots of $^1_\infty[MSe_3]$ and $^1_\infty[M_4Se_{10}]$ units, (4) differential thermal analysis (DTA) of **I**, **II**, **IV**, and **V**, (5) reconstructed image of [0*kl*] zone axis of **I**, (6) fractional atomic coordinates and equivalent isotropic atomic displacement parameters and site occupancies for **I**–**V**, (7) bond valence sums of M(4)–(6) in **I**, and (8) models of electronic structure calculation. These materials are available free of charge via Internet at http://pubs.acs.org.

■ AUTHOR INFORMATION

Corresponding Author

*E-mail: chishen@mail.nctu.edu.tw.

Notes

The authors declare no competing financial interest.

■ ACKNOWLEDGMENTS

We thank Professor Eric W.-G. Diau for measurements of UV diffuse reflectance. National Science Council (NSC98-2113-M-009-007-MY3) supported this research.

■ REFERENCES

(1) Kraemer, D.; Poudel, B.; Feng, H.-P.; Caylor, J. C.; Yu, B.; Yan, X.; Ma, Y.; Wang, X.; Wang, D.; Muto, A.; McEnaney, K.; Chiesa, M.; Ren, Z.; Chen, G. *Nat. Mater.* **2011**, *10*, 532.

(2) Sales, B. C. *Science* **2002**, *295*, 1248.

(3) Chung, D. Y.; Hogan, T.; Brazis, P.; Rocci-Lane, M.; Kannewurf, C.; Bastea, M.; Uher, C.; Kanatzidis, M. G. *Science* **2000**, *287*, 1024.

(4) Snyder, G. J.; Toberer, E. S. *Nat. Mater.* **2008**, *7*, 105.

(5) Rhyee, J.-S.; Lee, K. H.; Lee, S. M.; Cho, E.; Kim, S. I.; Lee, E.; Kwon, Y. S.; Shim, J. H.; Kotliar, G. *Nature* **2009**, *459*, 965.

(6) Mrotzek, A.; Iordanidis, L.; Kanatzidis, M. G. *Inorg. Chem.* **2001**, *40*, 6204.

(7) Mrotzek, A.; Chung, D.-Y.; Ghelani, N.; Hogan, T.; Kanatzidis, M. G. *Chem.—Eur. J.* **2001**, *9*, 1915.

(8) Mrotzek, A.; Kanayzidis, M. G. *Acc. Chem. Res.* **2003**, *36*, 111.

(9) Kanatzidis, M. G. *Acc. Chem. Res.* **2005**, *38*, 361.

(10) Ellis, J. Y. B. D. D. E.; Ibers, J. A. *Inorg. Chem.* **2002**, 7094.

(11) Assoud, A.; Derakhshan, S.; Soheilnia, N.; Kleinke, H. *Chem. Mater.* **2004**, *16*, 4193.

(12) Assoud, A.; Soheilnia, N.; Kleinke, H. *Chem. Mater.* **2004**, *16*, 2215.

(13) Assoud, A.; Soheilnia, N.; Kleinke, H. *J. Solid. State. Chem.* **2005**, *178*, 1087.

(14) Pocha, R.; Johrendt, D. *Inorg. Chem.* **2004**, *43*, 6830.

(15) Zelinska, M.; Assoud, A.; Graf, C.; Kleinke, H. *Inorg. Chem.* **2010**, *49*, 1090.

(16) Choi, K.-S.; Kanatzidis, M. G. *Inorg. Chem.* **2000**, *39*, 5655.

(17) Wang, Y. C.; DiSalvo, F. J. *Chem. Mater.* **2000**, *12*, 1011.

(18) Zhao, H.-J.; Li, L.-H.; Wu, L.-M.; Chen, L. *Inorg. Chem.* **2009**, *48*, 11518.

(19) Iordanidis, L.; Kanatzidis, M. G. *Angew. Chem. Int. ed* **2000**, *39*, 1928.

(20) Tampier, M.; Johrendt, D. *J. Solid. State. Chem.* **2001**, *158*, 343.

(21) Pocha, R.; Tampier, M.; Hoffmann, R. D.; Mosel, B. D.; Poettgen, R.; Johrendt, D. *Z. Anorg. Allg. Chem.* **2003**, *629*, 1379.

(22) Assoud, A.; Soheilnia, N.; Kleinke, H. *Z. Natur., Teil B. Anorgan. Chem., Organ. Chem.* **2004**, *59*, 975.

(23) Klepp, K. O.; Fabian, F. *Z. Kristallogr.—New Cryst. Struct.* **2002**, *217*, 475.

(24) Melullis, M.; Dehnen, S. *Z. Anorg. Allg. Chem.* **2007**, *633*, 2159.

(25) Huiyi, Z.; Fakun, Z.; Guocong, G.; Jinshun, H. *J. Alloys Compd.* **2008**, *458*, 123.

(26) Yu, C.-Y.; Wang, M.-F.; Chung, M.-Y.; Jang, S.-M.; Huang, J.-C.; Lee, C.-S. *Solid State Sci.* **2008**, *10*, 1145.

(27) Mrotzek, A.; Kanatzidis, M. G. *Inorg. Chem.* **2003**, *42*, 7200.

(28) Laugier, J.; Bochu, B. LMGP; Laboratoire des Materiaux et du Génie Physique de l'Ecole Supérieure de Physique de Grenoble. http://www.inpg.fr/, accessed September 2007.

(29) Han, J.; Spanheimer, C; Haindl, G; Fu, Ganhua; Krishnakumar, V; Schaffner, J; Fan, C.; Zhao, K.; Klein, A; Jaegermann, W *Solar Energy Mater. Solar Cells* **2011**, *95*, 816.

(30) *Bruker*; 2.1 ed.; Bruker AXS Inc.: Madison, WI, 2006.

(31) Skriver, H. L. *The LMTO Method*; Springer: Berlin, 1984.

(32) Andersen, O. K. *Phys. Rev. B* **1975**, *12*, 3060.

(33) van Barth, U.; Hedin, L. *J. Phys. C* **1971**, *4*, 2064.

(34) Blöhl, P. E.; Jepsen, O.; Andersen, O. K. *Phys. Rev. B: Condens. Matter* **1994**, *49*, 16223.

(35) Jepsen, O.; Andersen, O. K. *Z. Phys.* **1995**, *97*, 25.

(36) Dronskowski, R.; Blöhl, P. E. *J. Phys. Chem.* **1993**, *97*, 8617.

(37) Wang, Y. C.; Hofmann, R.; DiSalvo, F. J. *J. Solid. State. Chem.* **1999**, *159*, 230.

(38) Lychmanyuk, O. S.; Gulay, L. D.; Olekseyuk, I. D. *Pol. J. Chem.* **2006**, *80*, 463.

(39) Min, J.; Menghe, B.; Shouhua, J.; Yonglin, A. *Inorg. Chem. Commun.* **2007**, *10*, 555.

(40) Bangjin, G.; Crerar, S. J.; Mar, A.; Albrecht-Schmitt, T. E. *J. Solid. State. Chem.* **2006**, *179*, 1596.